Paper

# Application of Perfectly Matched Layer Absorbing Boundary Conditions for Propagation of Surface Wave on the Long Plasma Cable

Shamim Ahmad* Student Member
Kiyohide Baba* Non-member
Keiji Nakamura* Member
Shunjiro Ikezawa* Member

We have developed a computer code for the simulation of large scale SWP plasma excited by a long coaxial antenna with a VHF wave of 300 MHz, this antenna is located along the center axis of a cylindrical chamber. The antenna used in this model structure is so long that the computational region has become very large. Therefore, for the calculation of the electromagnetic field profile in order to design a long and large scale SWP plasma, it is necessary to apply a proper boundary condition to truncate the computational region, and from this viewpoint we have introduced the PML absorbing boundary conditions and have studied the effectiveness of this boundary conditions for our purposes.

**Keywords :** surface wave, plasma, finite element method, electromagnetic wave, perfectly matched layer, absorbing boundary condition

## 1. Introduction

Recently Surface wave produced plasma (SWP) has drawn much attention in processing of plasma as well as a large-area flat plasma source [1] [2]. Since it has been found that surface wave plays an important role in sustaining an overdense plasma [3], therefore, several works have been performed in this area [4] [5]. Usually for the computer simulation of surface wave produced plasma, the Finite Element Method (FEM) [6] or the Finite Difference Time Domain Method (FD-TD) [7] are employed.

In the case of the numerical simulation of electromagnetic field distribution in an axially symmetric chamber filled with plasma excited by VHF of 300 MHz by a long coaxial antenna in order to design a long plasma cable, the computational region has become very large. But either the element size in the FEM or shell size in the FD-TD method plays an important role to obtain more accurate result [8], therefore, applying either FEM or FD-TD method on a large computation region may be inconsistent with the speed and memory of a computer. As a result, for our problem, it was necessary to truncate the computational region and thus, an effective boundary condition was needed that permits all out-ward propagating numerical waves to leave problem domain as if the simulation were performed on a computational region of infinite extend. This type boundary conditions are either called radiation boundary condition [9] or absorbing boundary condition. In 1994, the approach was introduced by Berenger [10] to realize this Absorbing Boundary condition (ABC) is to terminate the outer boundary of the problem domain in an absorbing material medium, called the perfectly matched layer (PML). The invocation of Berenger's PML is that plane wave of arbitrary incident, polarization and frequency are matched at the boundary.

In the recent past, a lot of papers have been appeared describing the application of this PML absorbing boundary condition for different purposes [11]-[15]. With this background, we have applied the PML absorbing boundary condition in FEM for the analysis of surface wave propagation on a long SWP cable. For the iterative calculation to design a long SWP cable, in the first iteration, we have to start the calculation of electromagnetic field distribution by considering a constant electron density profile, but from the second iteration, electron density to be calculated from the electric field distribution obtained in the just previous iteration, and this iteration process should be continued until some convergence is reached. Therefore, it is necessary to study the validity of this PML absorbing boundary condition for both constant and density gradient plasma and it has been studied in our work.

In this paper, we will show the derivations of the equations for FEM and PML used in our plasma model, and will report the derived appropriate parameters of PML for better effectiveness.

## 2. The Equation of FEM and PML

Berenger [10] derived a novel split-field formulation of Maxwell's equation where each vector filed component is split into two orthogonal component. The original split-field concept was restated in stretched-coordinate form [7] [16], this extends the use of the PML to a cylindrical or spherical co-ordinate systems. By choosing loss parameters consistent with the dispersionless medium, a perfectly matched planner interface is derived.

Following this way, in our work, the PML material has been introduced in FEM to sustain the required boundary conditions. The outline of the model of our problem and the obtained equations are given below.

We have considered the geometry illustrated in Fig. 1, where a coaxial antenna covered by dielectric materials has been connected along the center axis of the cylindrical chamber filled with an axially symmetric plasma, this plasma is to be produced by the excitation of VHF wave of 300 MHz. This geometry is rotationally symmetric with respect to the axis of the antenna,

* Prof. Ikezawa Lab, Department of Electrical Engineering, Chubu University
1200 Matsumoto, Kasugai 487-8501

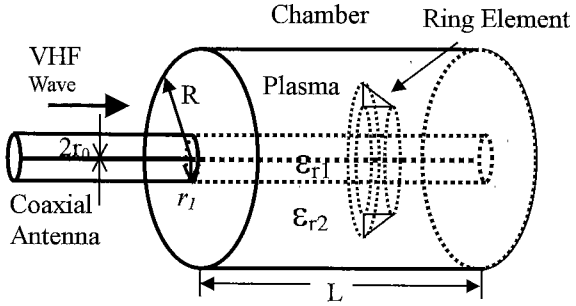


Fig. 1. Geometry of axially symmetric chamber

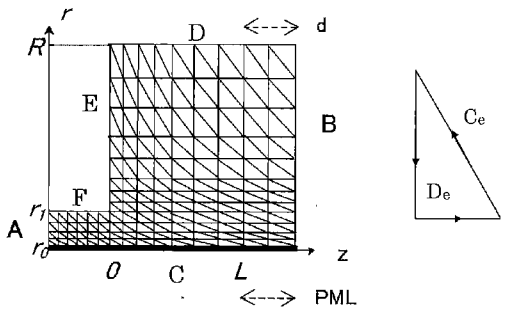


Fig. 2. Cross section of sample subdivision of elements for problem domain

therefore, we can analyze the axisymmetric problem, which is substantially two-dimensional in the *rz*-plane as shown in Fig 2. The governing equation is written for the incident transverse magnetic (TM) wave $(E_r, H_\theta, E_z)$ as,

$$\frac{\partial}{\partial r}\left\{\frac{1}{\varepsilon_r r}\frac{\partial}{\partial r}(rH_\theta)\right\}+\frac{\partial}{\partial z}\left(\frac{1}{\varepsilon_r}\frac{\partial H_\theta}{\partial z}\right)+k^2H_\theta=0 \quad \cdots\cdots (1)$$

and,

$$\left.\begin{aligned} E_r &= j\frac{1}{k\varepsilon_r}\frac{\partial H_\theta}{\partial z} \\ E_z &= -j\frac{1}{k\varepsilon_r}\frac{1}{r}\frac{\partial}{\partial r}(rH_\theta) \end{aligned}\right\} \quad \cdots\cdots (2)$$

where $H_\theta$ is the magnetic field intensity in θ direction, $E_r$ and $E_z$ are electric field intensity in radial and axial direction respectively and k is the wave number. In order to keep the dimension of the magnetic field same to the electric field, in the above equation we have considered $H_\theta \Rightarrow Z_0 H_\theta$, where intrinsic impedance $Z_0=120\pi$ [ohm]. Then, the weighted residual integration for the weighted functions has been set to zero and descried in the following,

$$\int_v w\left[\frac{\partial}{\partial r}\left\{\frac{1}{\varepsilon_r r}\frac{\partial}{\partial r}(rH_\theta)\right\}+\frac{\partial}{\partial z}\left\{\frac{1}{\varepsilon_r}\frac{\partial H_\theta}{\partial z}\right\}+k^2H_\theta\right]dv=0 \quad \cdots\cdots (3)$$

Here, w is the weighting function. Now, considering $\phi=rH_\theta$, $w=w_j$, $dv=2\pi r dr dz$ we get,

$$\sum_e \int_{D_e}\left[w_j\left\{\frac{1}{\varepsilon_r r}\frac{\partial\varphi}{\partial r}\right\}+\frac{\partial w_j}{\partial r}\frac{1}{\varepsilon_r}\frac{\partial\varphi}{\partial r}+\frac{\partial w_j}{\partial z}\frac{1}{\varepsilon_r}\frac{\partial\varphi}{\partial z}-k^2w_j\varphi\right]drdz$$
$$-jk\sum_{C_e}\oint\left\{(w_j rE_z)dz+(w_j rE_r)dr\right\}=0 \quad \cdots\cdots (4)$$

where, $D_e$ denotes cross section of the *e*-th ring element and $C_e$ denotes the contour enclosing $D_e$ *as* shown in Fig. 2. Now, solution of ϕ for e-th element is given by,

$$\varphi^e(r,z)=\sum_i \varphi_i^e N_i^e(r,z) \quad \cdots\cdots (5)$$

where, $\phi_i^e$ is a value of the ϕ at i-th node of e-th element, $N_i^e$ is the shape function of e-th element. Now, according the Galerkin method [6] weighting function should be equal to the summation of shape function, that is,

$$w_j=\sum_{e'} N_{j(e')}^{e'} \quad \cdots\cdots (6)$$

where, e′ means the number of elements which surrounds the globally numbered node *j*, from equation (4), (5) and (6), replacing $w_j$ *(j=1,2,...)* with shape function, we get

$$\sum_e \int_{D_e}\left\{\left[N^e\right]\frac{1}{\varepsilon_r r}\left[\frac{\partial N^e}{\partial r}\right]^T+\left[\frac{\partial N^e}{\partial r}\right]\frac{1}{\varepsilon_r}\left[\frac{\partial N^e}{\partial r}\right]^T+\left[\frac{\partial N^e}{\partial z}\right]\frac{1}{\varepsilon_r}\left[\frac{\partial N^e}{\partial z}\right]^T-k^2\left[N^e\right]\left[N^e\right]^T\right\}\left[\phi^e\right]drdz$$
$$-jk\sum_e \oint_{C_e}\left\{\left(\left[N^e\right][rE_z]\right)dz+\left(\left[N^e\right][rE_z]\right)dr\right\}=0 \quad \cdots\cdots (7)$$

where,

$$\left[N^e\right]=\left[N_1^e \ \cdots\cdots \ N_m^e\right]^T, \quad \left[\varphi^e\right]=\left[\varphi_1^e \ \cdots\cdots \ \varphi_m^e\right]^T$$

where, T denotes transpose of the matrix. We have employed second-order triangular ring element[6] to subdivide the problem domain, which means each element has six shape functions of second-order polynomials to describe the field quantities within the elements. $\varepsilon_{ri}$ (i=1 or 2) have also been represented by the second-order polynomials within the elements. Equation (7) gives the solution for e-th element, thus summing up for the all element, this equation will give the solution for the whole problem domain.

In the Fig. 2, all the sides except the side A and B, have been supposed as a conducting material, therefore, with this boundary condition, at all these sides tangential component of electric fields have been set to zero, that is, at side C, D and F in Fig. 2, the electric field component $E_z$ have been set to zero and at side E, electric field component $E_r$ has been set to zero. On the other hand, at side A of the chamber, impedance matching boundary condition has been applied, that is, at this side it has been set $E_r^r = ZH_\theta^r$, where, $E_r^r$ and $H_\theta^r$ are the radial component of reflected electric field and θ component of the reflected magnetic field, respectively and $Z=1/\sqrt{\varepsilon_r}$ where, $\in_r$ is the relative permitivity.

In the plasma medium, the relative permitivity $\in_r = \in_{r2}$ (as shown in Fig. 1) should be defined by the following equation[17],

$$\varepsilon_r = 1-\frac{\omega_p^2}{\omega^2\left(1-j\frac{\nu}{\omega}\right)} \quad \cdots\cdots (8)$$

where, $\omega_p=2\pi f_p$ and $f_p$ is the plasma frequency, ω is the frequency of the applied VHF and ν is the electron collision frequency, in our model ν/ω has been considered at 0.0015.

Now, VHF has been applied from the left hand side cross section A of the geometry of Fig. 2 and right hand has been supposed to be an infinite long chamber, at this side B, PML absorbing boundary condition has been set to truncate the

calculation area, outer side of this region has been considered as conducting material, and this region has been supposed to be perfectly matched and thereby, no reflection should be occurred from this PML region.

In the PML region, the relative permeability and permitivity are perfectly matched by a tensor [7] [15],

$$\tilde{\varepsilon}_r = \varepsilon_r \tilde{s}, \qquad \tilde{\mu}_r = \mu_r \tilde{s} \quad \cdots\cdots (9)$$

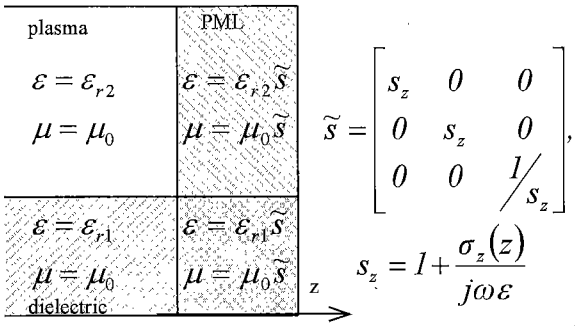


$\cdots\cdots (10)$

where, $\varepsilon_{ri}$ and $\mu_0$ are relative permitivity and permeability of the medium in which i=1 is for dielectrics and i=2 for plasma, $\varepsilon$ is the permitivity at PML's contact plane. In the PML region the equation (1) has been re-written and had to be solved. However, it should be noted here that the effectiveness of the PML material depends on it's conductivity and length.

## 3. Calculations and Result

The dimension of the considered geometry of our problem have been supposed as follows; radius of the antenna $r_0$=0.15 [cm], the thickness of dielectric material around the antenna ($r_1$-$r_0$)=0.35 [cm], radial length of the chamber R=14 [cm], axial length of the chamber OL=100 [cm] (see Fig. 2), width of the PML region d=10 [cm]. The total number of elements within the cable (outside chamber), chamber and PML region along z-axis is 25+250+25-=300 and the length of each element was 0.4 [cm]. Again, along r axis the total number of element was 41, the length of first element nearest to the central z-axis was 0.15 [cm], the length of each of next 12 was 0.175 [cm] and finally, length of each of the rest 28 was 0.4 [cm]. The relative permitivity of the dielectric material around the antenna $\in_r = \in_{r1}$ (as shown in Fig. 1) =2.3. The conductivity of the PML region $\sigma_z$ can be described by the following equation[18],

$$\sigma_z = \sigma_0 \left\{ \left( z - z_1 \right) / d \right\}^m \quad \cdots\cdots (11)$$

In Eq. (11), $m$ is the order of the polynomial, $\sigma_0$ is the maximum conductivity *in* PML region, $z_1$ is the starting point of PML region on z axis and $d$ is the width of PML.

The length of the coaxial cable outside the chamber has been considered at 10 [cm]. The frequency of the applied VHF of transverse electromagnetic (TEM) mode from side A of the chamber has been supposed at 300 MHz. The amplitude of the applied VHF $\phi = rH_\theta$ has been set to 1 [a.u].

In our simulation problem, the validity and effectiveness of the applied PML have been studied for three electron profiles, these are, constant electron density all over the problem domain, exponentially decreased along radial direction while constant along axial direction and exponentially decreased along axial direction while constant along radial direction, the obligation of considering these three electron density profiles has been explained in the introduction of this paper.

At the first, the constant electron density profile $n=10^{12}$ [/cc] has been considered for the calculation and the obtained magnetic field profile $\phi$=$rH_\theta$ for the r-z plane is shown in Fig. 3.

The Fig. 4 shows the same result but at different radial distances. In this calculations, the considered parameter of PML region were, $\sigma_0$=0.21 [mho/m] and m=2. In our problem domain, PML region has begun at an axial distance z=100 [cm] and width of that PML region d= 10 [cm]. From this two figures it is clear that, within 100 [cm] along z axis, at different radial distance the magnetic filed intensity is almost constant, which implies that the reflection is very low, but after entering into the PML region the magnetic field intensity has sharply become to zero, which implies that PML material has absorbed electromagnetic wave.

Now, in order to find out the optimal parameter of PML material, that is, the parameter at which the amplitude of the reflection should be minimum, at first, the arbitrary value of $\sigma_0$ has been kept constant at 0.21 [mho/m], and then the field profile for different value of polynomial order $m$ have been calculated, such a typical field profile at a radial distance r=0.35 [cm] is shown in Fig. 5. and respective percentage of reflections are tabulated in Table 1.

The Fig. 5 shows that a little standing wave exists and from Table 1, it is clear that the amplitude of the interference wave is minimum at the value of $m$=2. Since from Fig. 4 it has been found that after entering into the PML region the magnetic field intensity has become to zero, therefore, it could be concluded that

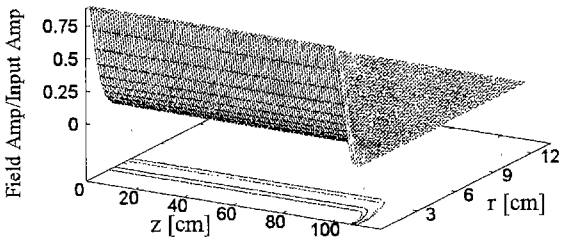


Fig. 3. Magnetic field $\phi$ ($=rH_\theta$) distribution within chamber ($d$=10 [cm], $\sigma_0$=0.21 [mho/m] and $m$=2)

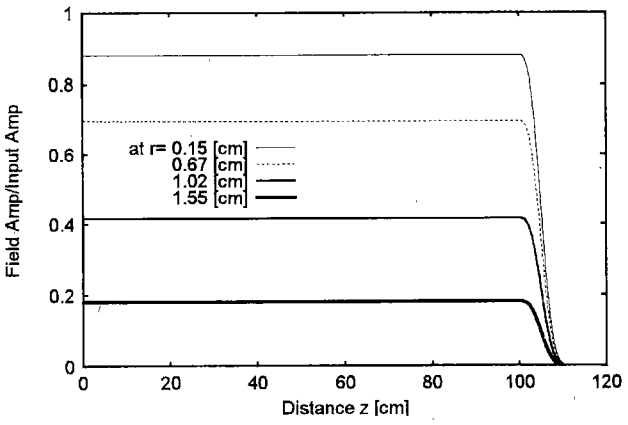


Fig. 4. Magnetic field intensity $\phi$ along $z$ direction at different radial distance $r$ ($d$=10 [cm], $\sigma_0$=0.21 [mho/m] and $m$=2)

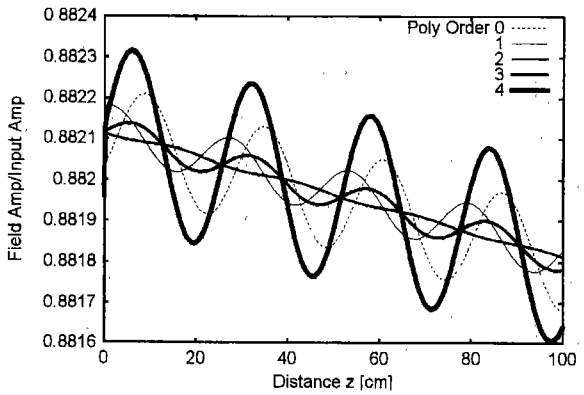


Fig. 5. Magnetic field intensity along $z$ direction for different polynomial order $m$; Electron density profile is constant $10^{12}$ [/cc] ($d$=10 [cm], $\sigma_0$=0.21 [mho/m] )

Table 1. Percentages of reflections for different polynomial order $m$ (Electron density profile is constant $10^{12}$ [/cc])

| $\sigma_0$ [mho/m] | Percentages of reflections [%] | | | | |
|---|---|---|---|---|---|
| | $m$=0 | $m$=1 | $m$=2 | $m$=3 | $m$=4 |
| 0.21 | 0.015 | 0.006 | 0.0003 | 0.0055 | 0.022 |

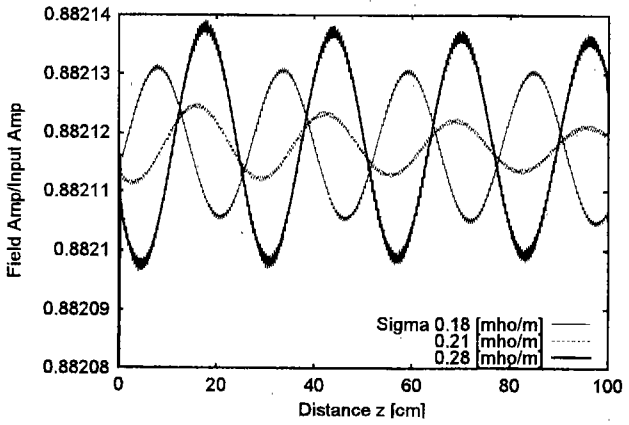


Fig. 6. Magnetic field intensity $\phi$ along $z$ direction of different 'maximum PML conductivity' $\sigma_0$. for constant electron density profile ($d$=10 [cm]and $m$=2)

these small standing wave shown in Fig. 5 are due to the reflection from the contact plane of PML material, thereby here impedance matching has been affected by the dispersion.

Now, keeping the value of the polynomial order constant at it's optimal value $m$=2 found just before, magnetic field profile for different value of $\sigma_0$ have been calculated, such a typical field profile at a radial distance r=0.5 [cm], that is, field profile on the dielectric surface is shown in Fig. 6 and the respective percentages of reflection has been tabulated in Table 2. The reason behind the noticeable difference between the form of Fig. 5 and 6 is that, to make Fig. 6 easier to understand of it's the amplitude of interference wave we are interested to, in this figure the slope of the intensity has been subtracted while slope of intensity of the wave of Fig. 5 has not been subtracted. However, from Fig. 6 and Table 2, it is clear that for $\sigma_0$=0.21 [mho/m] the amplitude of the interference wave is minimum.

Now, let us verify the effectiveness of PML absorbing boundary condition for exponentially electron density profile along radial and axial direction.

Table 2. Percentages of reflections for different sigma maximum $\sigma_0$ (Electron density profile is constant $10^{12}$ [/cc])

| Polynomial order m | Percentages of reflections [%] | | |
|---|---|---|---|
| | $\sigma_0$ = 0.18 [mho/m] | $\sigma_0$ = 0.21 [mho/m] | $\sigma_0$ = 0.28 [mho/m] |
| 2 | 0.0012 | 0.0003 | 0.0017 |

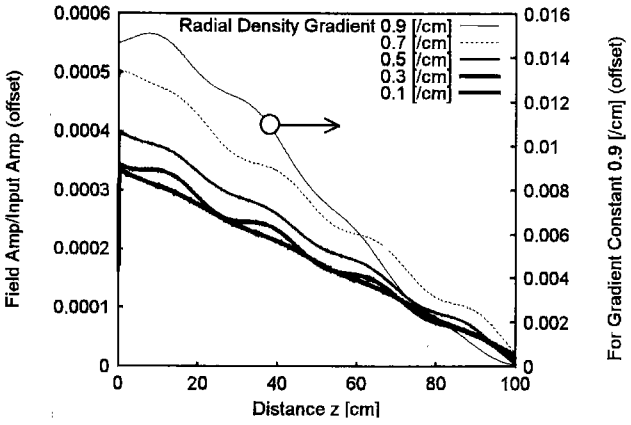


Fig. 7. Magnetic field intensity $\phi$ along $z$ direction for different electron density gradient in radial direction ($\sigma_0$= 0.21 [mho/m], m=2 and d= 10 [cm])

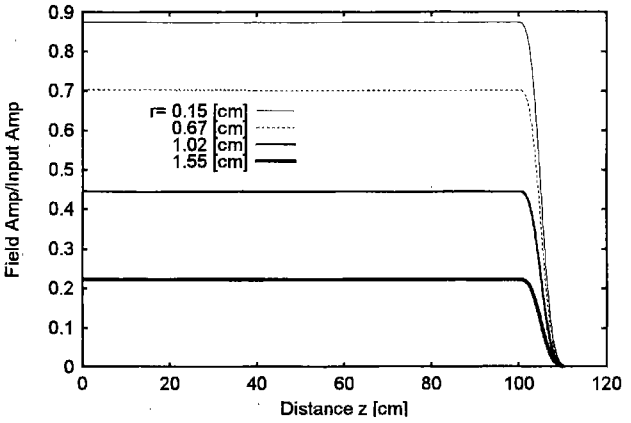


Fig. 8. Magnetic field intensity $\phi$ along $z$ direction at different radial distance $r$ for radial electron density Gradient 0.3 [/cm] ($d$=10 [cm], $\sigma_0$=0.21 [mho/m] and $m$=2)

Fig. 7 shows the magnetic field profile on the dielectric surface for an exponential electron density profile along radial direction for different electron density gradient while electron density profile along axial direction has been kept constant, in these cases, electron density on the antenna surface is $n_0=10^{12}$ [/cc], $\sigma_0$=0.21 [mho/cm] and PML width d=10 [cm]. In this figure at the point z=100 [cm] the minimum value of the field intensity along r axis has been set to zero by subtracting appropriate offset value. From this figure, it is clear that, the amplitude variation of magnetic field is small too, which implies that the electron density gradient in radial direction does not so much affect the PML conditions. However, here field amplitude is in decreasing nature since the electron density is in decreasing nature along radial direction.

Fig. 8 shows magnetic field intensity at different radial distance along z axis for a radial electron density gradient 0.3 [/cm]. This Figure shows that within the PML region field intensity has sharply become to zero that implies electromagnetic field has been

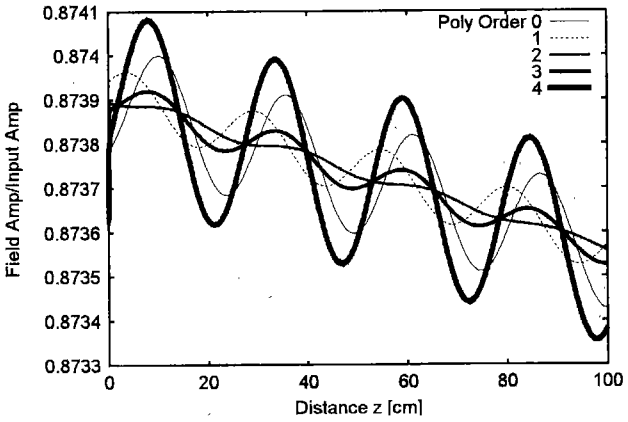


Fig. 9. Magnetic field Intensity along $z$ direction for different polynomial order $m$ ; Radial electron density profile is $10^{12}\times\exp(-0.3*r)$ ($d$=10 [cm], $\sigma_0$=0.21 [mho/m] )

Table 3. Percentages of reflections for different polynomial order $m$ (Radial Electron density profile is $10^{12}\times\exp[-0.3*r]$)

| $\sigma_0$ [mho/m] | Percentages of reflections [%] | | | | |
|---|---|---|---|---|---|
| | $m$=0 | $m$=1 | $m$=2 | $m$=3 | $m$=4 |
| 0.21 | 0.013 | 0.0065 | 0.001 | 0.004 | 0.021 |

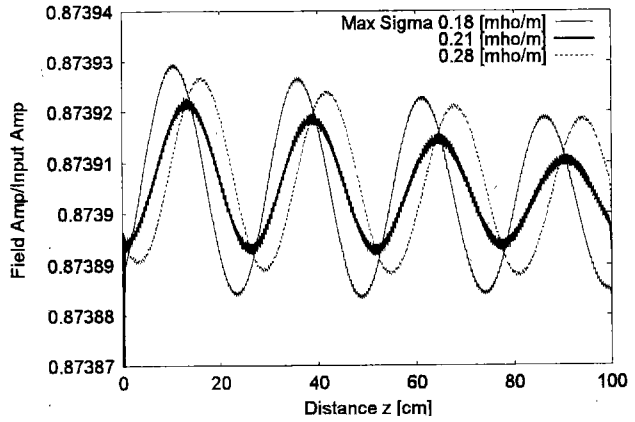


Fig. 10. Magnetic field intensity along $z$ direction for different $\sigma_0$ ; Radial electron density profile is $10^{12}\times\exp(-0.3*r)$ ($d$=10 [cm], Polynomial Order $m$ =2 )

absorbed in this region, Along with this, by following the same procedure as described in constant electron density profile case, it has been tried to find out the optimal PML parameters for the radial electron density profile case too.

A typical result for different polynomial order $m$ and sigma maximum $\sigma_0$ are shown in Fig. 9 and Fig. 10 respectively, and the respective percentage of reflections are also tabulated in Table 3 and 4,. from these two figures and two tables, it is clear that the optimal PML parameter for a PML width d=10 [cm] are m=2 and $\sigma_0$=0.21 [mho/cm], which are same as found for constant electron density profiles

Finally, exponential electron density along axial direction has been considered while along radial direction it has been kept constant, in these calculations, considered PML parameter were, width of PML d= 10 [cm], $m$=2 and $\sigma_0$= 0.21 [mho/m] and electron density profile $n_e$ was $n_0\times\exp(-\alpha z)$ [/cc], where, $n_0$ is the electron density at $z$=0 [cm] and $\alpha$ is the decaying constant. Fig.

Table 4. Percentages of reflections for different sigma maximum $\sigma_0$ (Radial Electron density profile is $10^{12}\times\exp[-0.3*r]$)

| Polynomial order m | Percentages of reflections [%] | | |
|---|---|---|---|
| | $\sigma_0$= 0.18 [mho/m] | $\sigma_0$= 0.21 [mho/m] | $\sigma_0$= 0.28 [mho/m] |
| 2 | 0.0016 | 0.001 | 0.0015 |

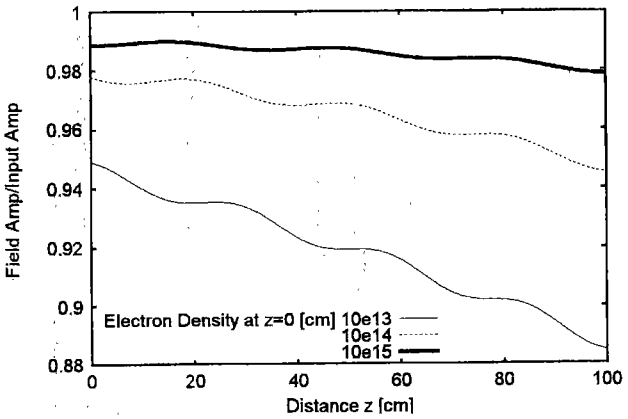


Fig. 11. Magnetic field intensity $\phi$ along $z$ direction for different electron density profile along axial direction ($\alpha$=0.023, $\sigma_0$= 0.21 [mho/m], $m$=2,and d= 10 [cm])

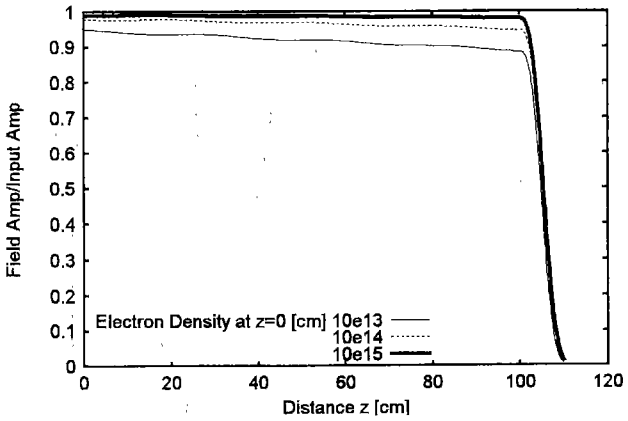


Fig. 12. Magnetic field intensity $\phi$ along $z$ direction at different radial distance $r$ for axially electron density profile ($\alpha$=0.023, $d$=10 [cm], $\sigma_0$=0.21 [mho/m] and $m$=2)

11 shows such a typical result within the chamber (0-100 [cm]) at radial distance r=0.5 [cm] for different electron density profile along z axis. Fig. 12 shows the same magnetic field profile but includes the PML region (0-110 [cm]) Figure 11 shows that the interference wave is larger in compare with the obtained field amplitude found for constant and radial electron density cases. Besides this, with this electron density model it has been found that the amplitude of the interference wave has not changed with the changes in PML parameter, rather has been affected by plasma impedance, that is, within chamber the amplitude of the interference wave is almost independent of PML material. A typical result describing that independency is shown in Fig. 13. But, from Fig. 12, it is obvious that after entering into the PML region the field amplitude has become to zero, which establishes the affectivity of PML boundary condition for this electron density model too.

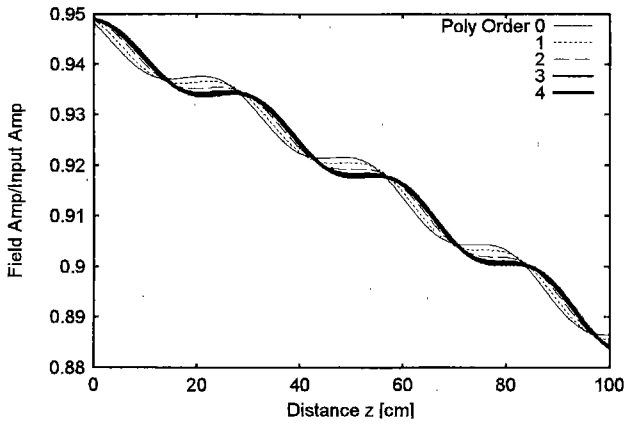


Fig. 13. Magnetic field intensity $\phi$ along $z$ direction at radial distance $r$=0.5 [cm] for axially electron density profile ($n_0=10^{12}\times\exp(-0.023*z)$ [/cc], $d$=10 [cm], $\sigma_0$=0.21 [mho/m])

Table 5. Percentages of reflection for different axial exponential electron density model ( $d$=10 [cm], $\sigma_0$=0.21 [mho/m] and $m$=2)

| Axial Electron Density profile $n_e=n_0\times\exp(-\alpha z)$ [/cc] | | | Percentage of reflections (%) |
|---|---|---|---|
| Electron density $n_0$ [/cc] at z =0 [cm] | Electron density [/cc] at z =100 [cm] | $\alpha$ | |
| $10^{13}$ | $1.35\times10^{12}$ | 0.02 | 0.2 |
| $10^{13}$ | $1.83\times10^{11}$ | 0.03 | 0.4 |
| $10^{13}$ | $4.97\times10^{11}$ | 0.04 | 0.4 |
| $10^{13}$ | $10^{12}$ | 0.023 | 0.3 |
| $10^{14}$ | $10^{13}$ | 0.023 | 0.21 |
| $10^{15}$ | $10^{14}$ | 0.023 | 0.11 |
| $10^{14}$ | $10^{12}$ | 0.043 | 0.7 |
| $10^{15}$ | $10^{12}$ | 0.069 | 1.0 |

Table 6. Results showing the effectiveness of PML boundary conditions applied in our model

| Width of PML d [cm] | Electron Density Profile | Polynomial Order m (Suitable Value Found) | Sigma Maximum $\sigma_0$ [mho/m] (Suitable Value Found) | Percentage of reflection [%] |
|---|---|---|---|---|
| 6 | Constant [$10^{12}$/cc] | 1 | 0.28 | 0.0125 |
| 10 | Constant [$10^{12}$/cc] | 2 | 0.21 | 0.0003 |
| | Radial Density Gradient $10^{12}\exp(-0.3\times r)$ | 2 | 0.21 | 0.001 |
| | Axial Density Gradient $10^{13}\exp(-0.023\times z)$ | No Effect in Changes | No Effect in Changes | 0.3 |

The percentages of reflection for different exponential axial electron density model are listed in Table 5. From this table, it should be concluded that for any electron density profile case like this present model where PML boundary condition is to be applied, in a suitable case reflection could be suppressed within 1%. At the last, it has been also studied the effectiveness of PML boundary conditions for different PML width, it has been found that changes in PML width changes the optimal value of polynomial order and 'sigma maximum $\sigma_0$' too, the obtained result for some typical cases are summarized in Table 6. From this table an important point should be noticed that percentages of reflection of the interference wave may not be same for all 'set of optimal PML parameter', therefore, it should take care to chose an appropriate PML width when PML boundary conditions is to be applied in such an application.

Beside these the effectiveness of element size has been studied for some typical cases in our calculation, for example, for the model of constant electron density $10^{12}$ [/cc] profile with PML parameter $m$=2, $\sigma_0$=0.21 [mho/cm] and $d$=10 [cm], we have calculated the field profile for two element size within chamber and PML region along z axis, those considered element size were 0.4 [cm] and 0.2 [cm], we have found almost same percentage of reflections for those both element sizes Therefore, the result we have until now will make it possible to apply suitable PML model to design a long SWP cable.

## 4. Conclusion

In order to truncate the calculation area for the simulation of long SWP cable, we have applied and studied the affectivity of the PML boundary condition for different electron density profiles. It has been found:

(1) PML is very effective for the model of constant electron density profile, where reflection has been suppressed within order of $10^{-5}$. In this model, the optimal PML parameter are $\sigma_0$=0.21 [mho/m] and $m$=2 for the value of d=10 [cm].

(2) For the model of exponential electron density profile along radial direction, PML is very effective too, In this model, the optimal PML parameter are $\sigma_0$=0.21 [mho/m] and $m$=2 for the value of d=10 [cm] as same found in the constant electron density model..

(3) For the model of exponential electron density profile along axial direction, little bit appreciable reflection has occurred at contact point of PML, in our model the value of this reflection was within 1%.

Therefore, in the iterative calculation for designing a long plasma cable, where a proper boundary is needed simultaneously for both constant and density gradient plasma to truncate the problem domain so that all out-ward propagating numerical waves are permitted to leave problem domain as if the simulation were performed on a computational region of infinite extend, the PML absorbing boundary condition can successfully be applied.

(Manuscript received Nov. 7, 2002, revised May 6, 2003)

## Reference

(1) I.P Ganachev and H. Sugai: "Production and control of planer microwave plasmas for material processing", *Plasma Sources Sci. Technol.*, Vol 11, pp. 178-190 (2002)

(2) T. Kimura, Y Yoshida, and S Mizuguchi : "Generation of a surface-wave-inhanced-plasma using co-axial-type open-ended dielectric cavity", *Jpn. J. Appl. Phys.*, Vol 34, No.8B, p. L1076 (1995)

(3) A.W. Trivelpiece and R. W. Gould . "Space charge waves in cylindrical plasma columns", *J. Appl. Phys.*, Vol.30, No.11, pp 1784-1793 (1969)

(4) M. Moisan, Z Zakrzewsky, R Pantel, and P Leprince : "A wave guide-based launcher to sustain long plasma columns through the propagation of an electromagnetic surface wave", *IEEE Trans. Plasma Science*, Vol.PS-12, No.3, pp. 203-214 (1984-9)

(5) Q. Chen, Poul H. Aoyagi, and M Katsurai . "Numerical analysis of surface wave ecitation in a planer-type nomagnetized plasma processing device", *IEEE Trans. Plasma Science*, Vol.27, No.1, pp 164-170 (1999-2)

(6) J. Jin · The Finite Element Method in Electromagnetic. John Wiley & Sons, Inc (1993)

(7) A. Taflove and S.C. Hangness : Computational Electrodynamics: The

Finite-Difference-Time Domain Method, 2nd ed. Artech House, Boston (2000)
(8) M. N. O. Sadiku . Numericals in Electromagetics, 2nd ed., p. 163, 424, CRT Press, New York
(9) T G Moore, J.G. Blaschak, A. Taflove, and G.A. Kriegsmann : "Theory and application of radiation boundary operators, IEEE Trans. Antennas Propagat.", Vol.36, pp. 1797-1812 (1988-12)
(10) J.P. Berenger · "A perfectly matched layer for absorption of electromagnetic waves", *J. Comput. Phys.*, Vol 114, pp. 185-200 (1994)
(11) J C Veihl and R. Mittra . "An efficient implementation of Berenger's Perfectly Matched Layer (PML) for Finite-Difference-Time–Domain mesh truncation", *IEEE Microwave Guide Wave Lett.*, Vol.6, pp. 94-96 (1996)
(12) M.F. Pasik, G. Aguirre, and A.C. Cangellaris : "Application of the PML absorbing boundary conditions to the analysis of patch antenna, *Electromagnetics*, Vol 16, pp. 435-449 (1996)
(13) S.D. Gednuy : "An anisotropic PML absorbing media for FD-TD simulation of fields in lossy depressive media", *Electromagnetics*, Vol.16, pp. 399-415 (1996)
(14) Q.H. Liu: "An FD-TD algorithms with perfectly matched layers for conductive media", *Microwave Opt. Tech. Lett.*, Vol.14, pp. 134-137 (1997)
(15) Z.C Sacks, D.M. Kingland, R.Lee, and J.F Lee: "A perfectly matched anisotropic absorber for use as an absorbing boundary condition", *IEEE Trans. Antennas & Propagat*, pp.1460-1463 (1995)
(16) W. C. Chew, J. M. Jin, E. Michielssen, and J. Song, ed. : Fast and Efficient Algorithms in Computational Electromagnetics, Artech House Publisher, Boston (2001)
(17) A. Ishimaru : Electromagnetic Wave Propagation, Radiation and Scattering, Englewood Chiffs, Prentice Hall, NJ (1991)
(18) J. P. Berenger : "Perfectly matched layer for the FDTD solution of wave-structure iteration problems", *IEEE Trans. Antennas & Propagat.*, Vol.51, pp. 39-46 (1996)

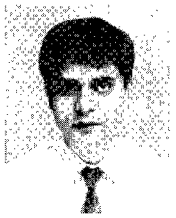

**Shamim Ahmad** (Student Member) is a PhD student in the department of electrical engineering of Chubu University, Japan. He received his M.Sc. degree in applied physics and electronics from Rajshahi University, Bangladesh and joined as a lecturer in the department of computer science of same university. Later he was a research student in the department of computer engineering of Inha University, Korea. His current research interests are simulation, algorithms, graphics and artificial intelligence. He is a member of Bangladesh Computer Society and IEEJ.

**Kiyohide Baba** (Non member) received his PhD in electronics engineering from Nagoya Institute of Technology. Now he is a professor in the department of electrical engineering of Chubu University. His current research interests are ELF and VLF radio wave propagation in the ionosphere and exosphere and surface wave plasma. He is a member of The Institute of Electronics, Information and Communication Engineers, Society of Geomagnetism and Earth, Planetary and Space Science

**Keiji Nakamura** (Member) received his PhD in electrical engineering from Nagoya University. Now he is an associate professor in the department of electrical engineering of Chubu University. His current research interests are production, diagnostics and control of high-density plasma sources, plasma-based materials processing, plasma application for environmental conservation, development of superconducting electric devices. He is a member of The Institute of Electrical Engineers of Japan, The Japan Society of Applied Physics, The Japan Society of Plasma Science and Nuclear Fusion Research, The Institute of Electrical and Electronic Engineering

**Shunjiro Ikezawa** (Member) received his PhD in electrical engineering from Nagoya University. Now he is a professor in the department of electrical engineering of Chubu University. His current research interests are new EBEP (Electro Beam Excited Plasma) apparatus, TiO2 Film, silicon film, New SWP (Surface Wave Plasma), poly-Si etching, DLC film. He is member of The Institute of Electrical Engineers of Japan, The Japan Society of Applied Physics, The Institute of Electronics, Information and Communication Engineers, The Japan Society of Plasma Science and Nuclear Fusion Research, The Physical Society of Japan